Optimization and Analysis of the Hydrodynamic Coefficients for an Underwater Vehicle (UV)

AICHA SEDINI[1]*, FETHI SAIDI[2], ABDELLAH MOKHTARI[2], ZAKARYA LAFFANE[2]
[1]Automatic Department
[2]Maritime Department
Aero-Hydrodynamic Naval Laboratory
University of Science and Technology M-B
1505 El'M'Naouer, 31000 Oran
ALGERIA
*Email: aicha.sedini@univ-usto.dz

Abstract: - The present paper achieves a numerical study to improve the performance of an optimal hull of an underwater vehicle using iso-geometrics equations of the model SUBMARIN hull and ANSYS CFX software package for Computational Fluid Dynamics. The study is twofold. First, evaluate and calibrate the CFD model for the underwater vehicle, second, the previous concept are transferred in order to obtain numerical results for AUV optimization and analysis. Optimization results for compliance criterions which allow controlling the shape such as drag coefficient is presented. The numerical results show a good agreement with those of the experimental one. Thus, an analysis of the coefficients of the added masses coefficients and the damping force are carried to help to understand the AUV acceleration behavior at sea.

Key-Words: - Underwater vehicle - hydrodynamic - added mass - optimization - CFD - boundary conditions

1 Introduction

The investigation of the underwater environment concerns many fields such as oceanographic research, military applications and recently offshore construction. In order to discover the seabed, underwater gear has been developed. Today, underwater robots such as Remotely Operating Vehicles (ROVs), Autonomous Underwater Vehicles (AUVs) are an integral part of scientific equipment to explore the seas and oceans. These vehicles are confronted to some major classes of scientific problems such as: decision-making autonomy, navigation coupled with the problem of positioning and energy autonomy. The latter consists to studying the hydrodynamic performance of this gear.

The hydrodynamic performance of an AUV system is a part of optimizations studies. Different configurations have been investigated in previous experimental and numerical studies. Among these studies, in 2008, Mashud Karim et al.[1] has demonstrate the efficiency of the shape on the drag forces by comparing the length to diameter ratios (L/D) for a flow around six axisymmetric AUV bodies. Furthermore, X li [2], KM tan [3] and Lihong Wu [4] discusses the dynamics of autonomous underwater vehicles (AUV) by modeling and evaluating hydrodynamic performance using the finite volume method based on the RANS (Reynolds Average Navier-Stokes) equations to compute the viscous drag. These research works have been enhanced by the experimental analyses of MSM Aras [5], R li [6], Gliu [7] and Mitra [8].They compares real-time scenario data with simulated data using the CFD models. Recently, the number of AUV has increased for sea depth exploitation, that can cause uncontrollable motions which may even cause the collision of the vehicles and lead to the failure of the mission, in this context, the interaction of many AUV shapes has investigated by Alexander Phillips and al 2013 [9], it studied experimentally the advancement resistance of an AUV by testing the effect of the pitch between three existing AUV bodies for different shape and size. On the other hand, Pareecha [10] and Yaxing [11] studied the influence of the depth of immersion of the AUV on its hydrodynamic behavior, for that, it used the cavitation number in these calculations. With regards to hydrodynamics forces, the drag force is not the only the influence on an AUV, whereas, the added mass affects all hydrodynamic motions such as the Surge, Sway and Yaw. These last are numerically investigated through the works of Guijie [12] and Haibin [13].

This paper is two cases. First, evaluate and calibrate the CFD model for the underwater vehicle using an

experimental work of Ting Gao and al [14]. Second, the previous concept is transferred in order to obtain numerical results for AUV optimization and analyses.

2 Numerical Modeling

The Geometric optimization of an UV using a CFD code is a complex process due to the turbulence flow around this vehicle, however it is necessary to prepare the mesh and calibrate it with the closure model. A preliminary study was developed in case (I) based on the experimental work of Ting Gao and al [14] in order to adapt the mesh with the model.

After the CFX code evaluation, the main part of this paper begins. Eight geometries are realized by ICEM with different nose and tail, a common middle with fixed dimensions (Table I). These shapes are compared with each other through the drag coefficient (Cd). The optimum UV design is examined and analyzed.

The same shape parameters [15] are used in both investigation (code evaluation (I) and the optimization (II)) and analysis.

2.1 Geometry and Domain Definition

The design of hull of an UV can be composed of three parts, namely the nose (a), the middle (b) and the tail (c). The UV form was designed by Myring Equations [15].

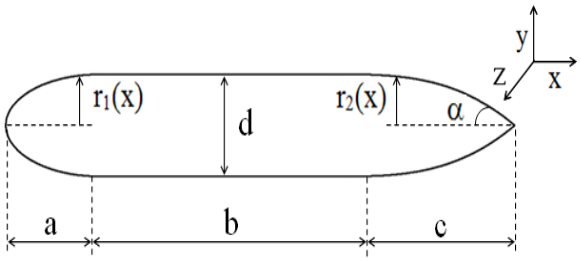

Fig.1: AUV parameters of Myring Equation

The geometry of the UV is axisymmetric and is shown in Figure 1. The parameterized shape of the body is given by:

$$r_1(x)=\frac{1}{2}d\left[1-\left(\frac{x-a}{a}\right)^{1/n}\right] \quad (1)$$

$$r_2(x)=\frac{1}{2}d-\left[\frac{3d}{2c^2}-\frac{\tan(\alpha)}{c}\right](x-(a+b))^2+\left[\frac{d}{c^3}-\frac{\tan(\alpha)}{c^2}\right](x-(a+b))^3 \quad (2)$$

Where x is the position along the rotation axis, r_1 and r_2 is the radius at a specific x, a is the length of the nose, b the length between nose and tail, c the length of nose, d is the diameter of UV and a circular cone has an angle α.

The geometric characteristics of UVs used in both parts of this paper are presented in table 1:

Table 1. UV Dimension Parameters

	(I) UV for CFX evaluation [Ting Gao and al.]	(II) UV optimization
Parameter	Value [m]	Value [m]
a	0.280	0.215
b	0.737	1.155
c	0.504	0.430
d	0.280	0.200

As shown in figure 2, a rectangular computational domain is chosen to avoid the flow return effect. It is extended up to *1L* upstream from the leading edge and *3L* downstream from the trailing edge; *7d* as the domain height and *3d* as width.

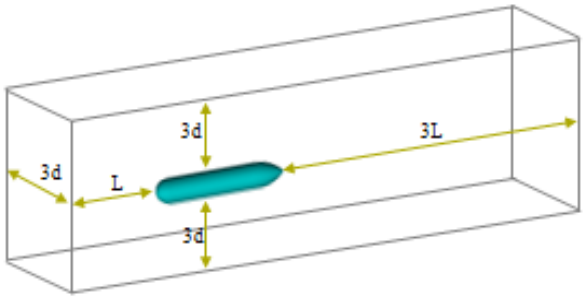

Fig.2: Computational domain

2.2 CFD Validation

In order to validate the appropriate mesh and CFD analysis we used the geometry of Ting Gao that was experimentally realized (table 1-part (I)).

2.2.1 Mesh Assessment

As shown in Figure 3, two types of structured and unstructured mesh controlled by physics and using hexahedral and tetrahedral elements respectively used to mesh the geometry to obtain the best possible results.

Mesh refinement was performed adjacent to the wall using the boundary layer mesh option, resulting in seven layers structured grid in the wall region.

The boundary conditions involved the adjustment of the incoming velocity distribution, without slip conditions on the hull wall of the vehicle, open boundary conditions without viscous shear at the far-side wall (outer *xy* plane), a symmetry flow condition along the *xz* plane through the origin and by the *yz* plane an exit condition was applied at the wall behind the vehicle.

(a)

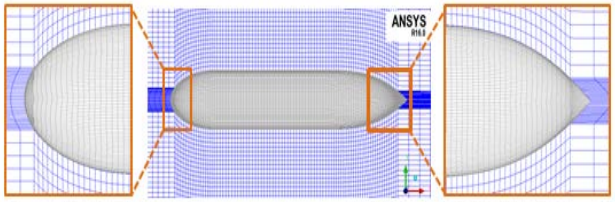

(b)

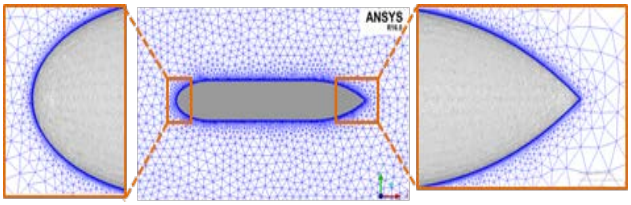

Fig.3: (a) Structured (Hexa, with 1640669 elements) and (b) unstructured (Tetra, with 1650374 elements)

2.2.2 Turbulence Model

The choice of the appropriate turbulence model is important for the underwater studies [16].
As proved by Jagadeesh et al in 2009 [17], the kε model is the better to predict the hydrodynamics coefficients and the boundary layer treatment and compared well with experimental data.
The kε turbulence model is a two-equation model that uses transportation equations to determine the balance of the kinetic energy of the fluctuations (k) and the energy dissipation (ε) [18].
The governing equations of the flow and the kε closure model used in this investigation can be written as follow:

- Continuity equation

$$div(\vec{U})=0 \Leftrightarrow \frac{\partial U_i}{\partial x_i}=0 \quad (3)$$

- Momentum equation

$$U_j\frac{\partial U_i}{\partial x_i}=-\frac{1}{\rho}\frac{\partial P}{\partial x_i}+\frac{1}{\rho}\frac{\partial}{\partial x_j}\left(\mu\frac{\partial U_i}{\partial x_j}\right) \quad (4)$$

- Medium continuity equation

$$\frac{\partial \overline{U}_i}{\partial x_i}=0 \quad (5)$$

- And the average momentum equation

$$U_j\frac{\partial U_i}{\partial x_i}=-\frac{1}{\rho}\frac{\partial P}{\partial x_i}+\frac{1}{\rho}\frac{\partial}{\partial x_j}\left(\mu\frac{\partial U_i}{\partial x_j}-\rho\overline{u_i u_j}\right) \quad (6)$$

The $K\varepsilon$ turbulence model is a two-equation model that uses transportation equations to determine the balance of the kinetic energy of the fluctuations (K) and the energy dissipation (ε). The equations in the model are given as,

- For the kinetic energy of the fluctuations (K)

$$\frac{\partial}{\partial t}(\rho k)+\frac{\partial}{\partial t}(\rho k u_i)= \frac{\partial}{\partial t}\left[(\mu+\frac{\mu_t}{\sigma_k})\frac{\partial k}{\partial x_j}\right]+p_K+p_b-\rho\varepsilon-Y_M+S_k \quad (7)$$

- For the energy dissipation (ε)

$$\frac{\partial}{\partial t}(\rho\varepsilon)+\frac{\partial}{\partial t}(\rho\varepsilon u_i)= \frac{\partial}{\partial t}\left[(\mu+\frac{\mu_t}{\sigma_\varepsilon})\frac{\partial \varepsilon}{\partial x_j}\right]+C_{1\varepsilon}\frac{\varepsilon}{k}(p_K+C_{3\varepsilon}p_b) -C_{2\varepsilon}\rho\frac{\varepsilon^2}{k}+S_\varepsilon \quad (8)$$

Where S is the modulus of the mean rate of strain tensor, $C_{1\varepsilon}=1.44$, $C_{2\varepsilon}=1.92$, $C_{3\varepsilon}=0.33$, $\sigma_k=1.0$, and $\sigma_\varepsilon=1.3$.

The boundary conditions used by Ting Gao and al [14] in his experimental study show that the Reynolds number is of the order which requires activation of the turbulence modeling.

Table 2. Experimental and predicted drag forces

Velocity (ms^{-1})	Drag force Ting Gao and al, 2017 (N)	Drag force present study (N)	
		Hexa mesh	Tetra mesh
0.3	0.273642	0.302387	0.322882

According to table2 above, comparing the predicted drag force for a velocity of 0.3(ms^{-1}) with the experimental of Ting Gao and al [14], the structured mesh (hexa) give a better precision than the unstructured mesh (tetra).

The independence of the mesh solution was checked, and mesh quality was assessed with the values of the pressure coefficient (Fig. 4). There is a slight difference between the results of *Cp* obtained by the two meshes and it is due to the refinement near the wall.

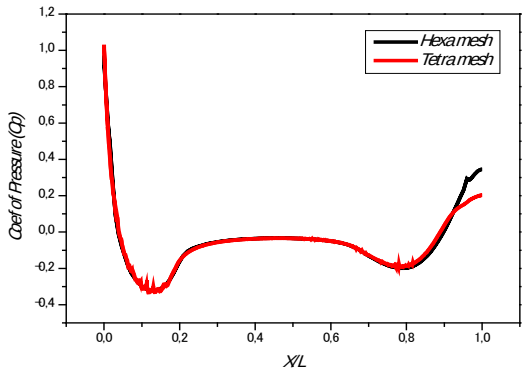

Fig.4: Pressure coefficient comparison for tetra and hexa meshes

2.2.3. Model Evaluation

Figure 5 indicates that the experimental drag force is in good agreement with the drag force modeled with reversal of superiority noted after the Reynolds number 3.10^6.

In carrying out the current analysis, baseline computations were carried out with the hexa grid combined to Kε model for comparison. The comparison showed that this system combination model is better to continue the optimization and the investigation; hence it was adapted for the computations.

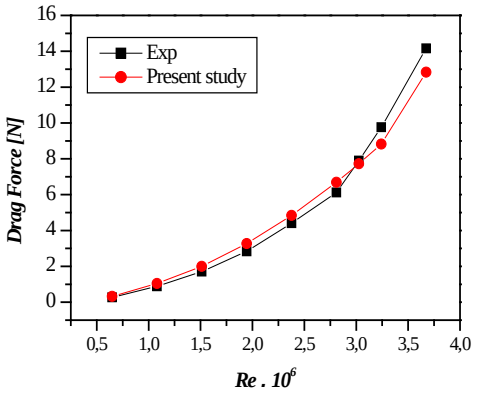

Fig.5: Model evaluation for the predicted and experimental drag forces

3 AUV Optimization

The optimization methodology is illustrated in figure 6. The chosen optimization variable is the drag hydrodynamic factor, which allow controlling the shape

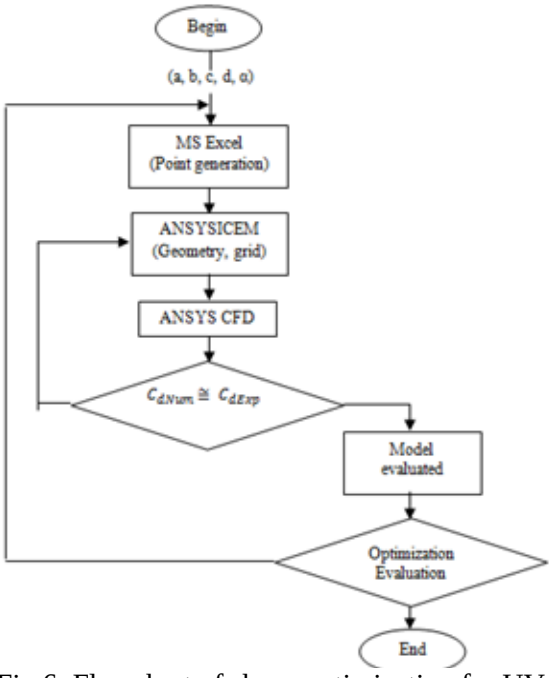

Fig.6: Flowchart of shape optimization for UV

3.1 Geometry and Mesh Generation

The UV design is based on equations 1 and 2 using the dimensions of each part mentioned in the table 1. However, eight geometries were evaluated for different shapes by varying the number n and α from 1 to 4 with a step of one and from 15° to 30° with a step of 5° respectively (Fig 7-a and b) in order to carry the optimum UV shape

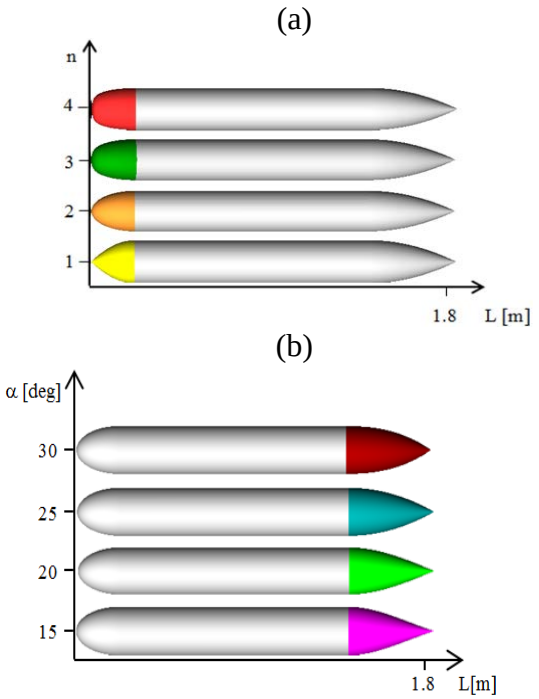

Fig.7: Vehicle shapes for different parameters of n (a) and α (b)

As indicated above, the domain size and the combined system (Hexa mesh size of order *1841474* elements and k eps model) proved its ability to predict a good hydrodynamic force.

With this conclusion, a similar condition of the combined system has been calibrated for the optimization and the analysis (Fig.8.).

.

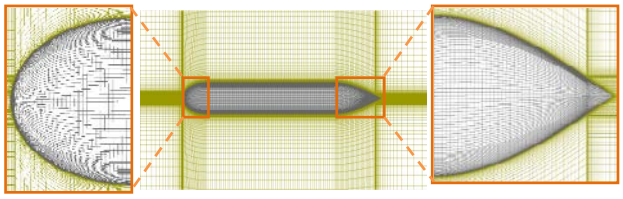

Fig.8: Hexa meshes of the UV

4 AUV Results and Discussion

Simulations were carried out under the conditions mentioned before, in order to calculate the drag force for eight forms of UV geometries and to determine the influence degree of each form with respect to the others, as well as the visualization of pressure coefficient of each case.

4.1 Calculation and Optimization of the UV

4.1.1 Drag Coefficient

The drag caused by an axi-symmetric UV moving forward under the water is a direct result of the viscosity of the water.

Figure 8 shows drag coefficient estimates for the eight vehicle shapes that were considered during the CFD optimization study, i.e. drag coefficient evolution for different *n (a)* and *α (b)*. The simulation results indicate that the minimum *Cd* is noted for *n=2* and *α=20°*.

(a)

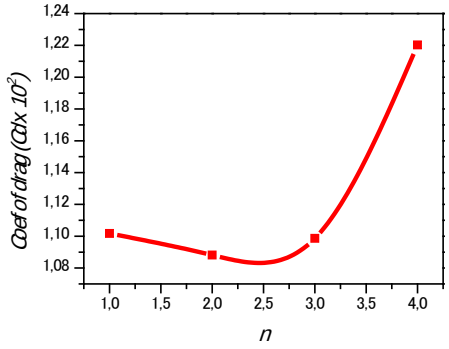

(b)

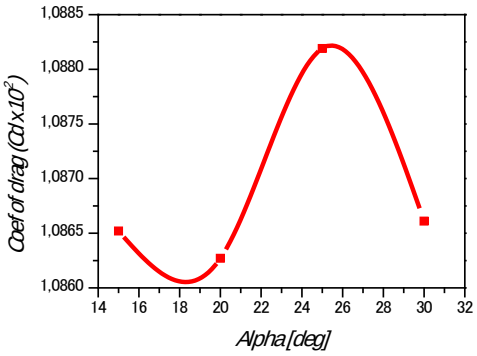

Fig.9: Drag coefficients of different value of n (Fig (a)) and the angle α (Fig (b))

4.1.2 Pressure Coefficient

In order to confirm the accuracy of the optimization results, the pressure coefficients *Cp* according to UV length are visualized in Figure 8. According to these results the variation of *Cp* is clearly influenced by the shape of the nose a little less for the tail form. A pressure distribution variation at the tail is noted, this is due to the nose leading-edge form, whereas, the shape of the tail does not change the pressure distribution of the on the hull of the UV. However, the most favorable geometry is that of the combined of *n=2* with *α= 20* according to the pressure distribution.

(a)

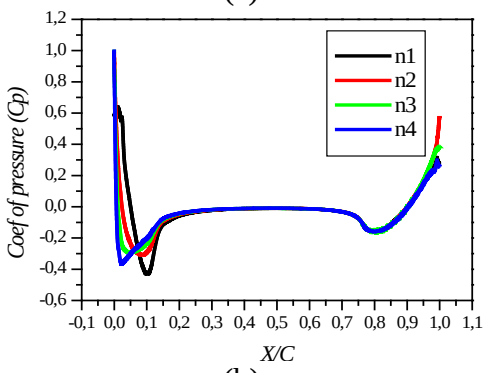

(b)

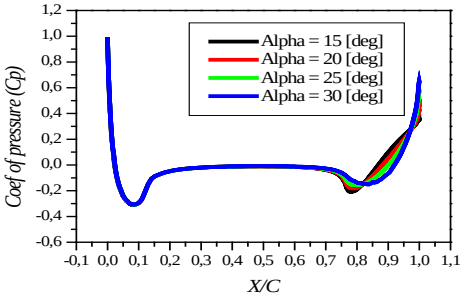

Fig.10: Cp distribution around the UV for n (a) and α (b)

According to CFD results, the optimum hull geometry was found, and therefore the UV with $n=2$ and $\alpha=20$ is the best shape;
This optimum shape is named ***UV-LAHN***.

4.2 Optimum UV-LAHN Investigation

4.2.1 Drag Coefficient

Table 3 shows the validation of the drag coefficient by experimental results. Drag values for the UV-LAHN model at Reynold number of $2{,}3.10^7$ was calculated through CFD code and compared to experimental works. According to this results we note that the *Cd* obtained during this simulation is in good agreement with that of experimental, in the same context one can note a difference between the present study and that of White [19], Baker [20] and Karim [1].This is due to the mesh choice as well as the closure model used in this case.

Table 3. Drag
G

	Cd Exp White, N.M, 1977	Cd Baker, C, 2004	Cd MM. Karim and al, 2008	Cd Present study
Re = 2,30x10^7	0,00123 ±0.000314	0.00167	0.00104	0.00108

4.2.2 Velocity Profile

The figure 10 shows the variation of the flow velocity through *xy* plan. The evolution of the boundary layer along the walls of the computational domain has been well predicted. In addition, the wake development downstream of the UV has been correctly captured.

One can also note that the realistic prediction of the acceleration of the fluid at the reduced sections between UV and the walls of the domain.

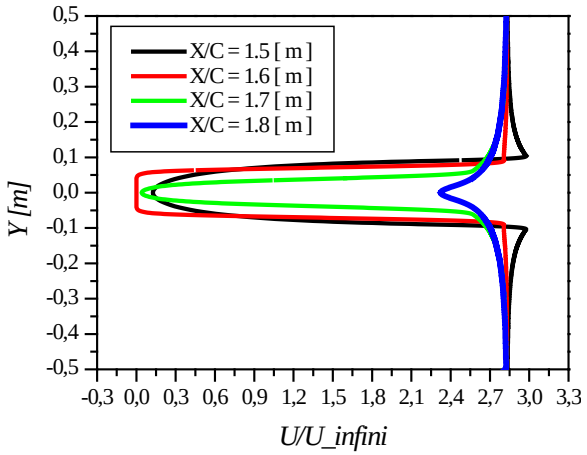

Fig.11: Velocity profil in XY plane

4.2.3 Added Mass and Damping Force

The added mass is a movement effect of the water on the UV. Therefore, the effect of viscosity can be considered as two separate factors. The first one is the skin friction which is caused by viscosity shear force of a fluid flowing along the hull, and the other is the form drag caused by development of a boundary layer and the resulting difference of pressure distribution between front and stern of the vehicle.

Table 4. Add mass formulation

DOF	MOTION DESCRIPTION	EQUATION	
1	Surge (Motions in the x-direction)	λ11=Fx/Ax	(9)
2	Sway (Motions in the y-direction)	λ22=Fy/Ay	(10)
3	Yaw (Rotations in the z-direction)	λ26=My/Ay	(11)

The figure 11 shows the variation of UV-LAHN for the added masses λ_{11}, λ_{22}, λ_{26} immersed in water Reynold number.

The added mass of the three components, calculated using ANSYS CFX, perfectly reflects the effect of translation and rotation in the three directions.

An inverse relationship between the coefficients of the added mass and the acceleration is noted, i.e. an increase in acceleration causes a decrease in coefficients of added mass (eq 9, 10, 11).

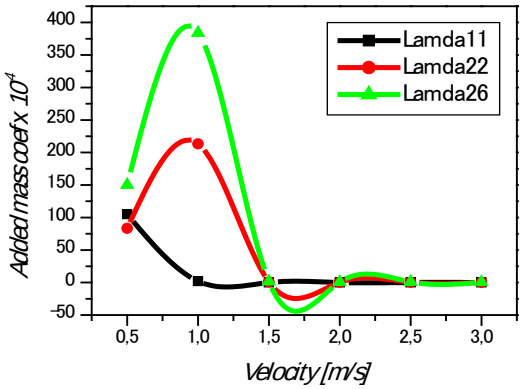

Fig.12: Added mass coefficients

The damping forces and moments act on any moving body in a supposed viscous fluid. They are due to the action of the added mass of water and the viscous friction of the fluid on the moving body. Assuming that the vehicle rotates uniformly around the specified center, the distance between vehicle centroid and circular motion center is given by R,

hence the hydrodynamic forces can be formulated as follows [11]:

$$qSC_{y1}(\alpha) + qSC_{y1}(\omega_{z1}) \approx qSC_{y1}^{\alpha}\alpha + qSC_{y1}^{\overline{\omega_{z1}}}\overline{\omega_{z1}} = N + \lambda_{11}V\omega_{z1}\cos\alpha \quad (12)$$

$$qSlm_{z1}(\alpha) + qSlm_{z1}(\omega_{z1}) \approx qSlC_{m_{z1}}^{\alpha}\alpha + qSlC_{m_{z1}}^{\overline{\omega_{z1}}}\overline{\omega_{z1}} = M + \lambda_{26}V\omega_{z1}\cos\alpha + (\lambda_{22} - \lambda_{11})V^2\sin\alpha\cos\alpha \quad (13)$$

Where the notation *N* and *M* are the normal force and pitch moment, the rotating$\omega_{Z1}$is the angular speed, the velocity at vehicle centroid will be $V = R\omega_{z1}$, the damping force coefficient is$C_{y1}^{\overline{\omega}_{z1}}$and the pitch damping moment coefficient is$C_{m_{z1}}^{\overline{\omega}_{z1}}$.

Figure 12 show the hydrodynamic force witch the increase depends on the velocity increasing. The figure shows a logical result comparing with the work of Chin [21].

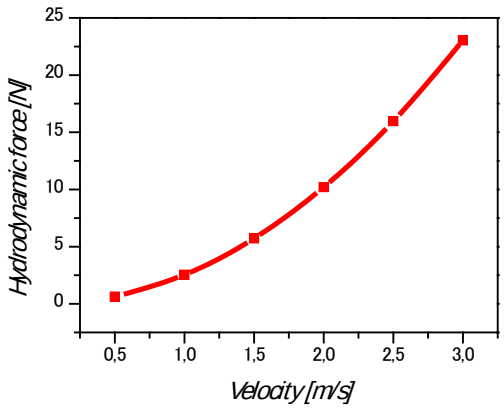

Fig.13: Hydrodynamic damping force

5 Conclusion

This article deals with the optimization of a better form of a submarine (UV-LAHN) using a hydrodynamic performance analysis obtained from a digital investigation.

In this context, this study is divided into two part as follows:

1- Model calibration for submarine, mesh and boundaries conditions adaptation

2- Shape optimization, comparison and the choosing of the best form according to the drag coefficient. Whereas, the hydrodynamics performances (*Cd*, λ_{11},λ_{22},λ_{26}, and damping force) of optimum UV were analyzed

According to the drag force results comparison for many velocities, a good agreement was noted for the drag forces. The CFD can predict the hydrodynamics forces for submarine vehicles. However, the CFD optimization part of this paper revealed that $n = 2$ and $\alpha = 20$was the optimal shape (UV-LAHN) by the confrontation of *Cd* for the eight submarines geometries;

The numerical investigation on the UV-LAHN showed that the added masses values is a smaller order for the velocities tested, which explains the low value of the drag force, in addition, the damping force linearity indicate that the optimal submarine UV-LAHN has a good hydrodynamics form.

References

[1] M. Karim, Numerical Computation of Viscous Drag for Axisymmetric Underwater Vehicles, *Journal Mekanikal*. Vol. 26, n. 2, 2008, pp.9 – 21.

[2] X. Li, M. Zhao, FM. Zhao, QQ. Yuan, T. Ge, Study on hydrodynamic performance of Heavier-than-water AUV with overlapping grid method, *Ocean Syst Eng*. Vol. 4,n. 1, 2014, pp.1–19.

[3] KM. Tan, T. Lu, F. Tien, A. Anvar, Drag coefficient estimation model to simulate dynamic control of autonomous underwater vehicle (AUV) motion, *20th International Congress on Modelling and Simulation*, 2013, pp. 1–6.

[4] L. Wu, Y. Li, S. Su, p. Yan, Y. Qin, Hydrodynamic analysis of AUV underwater docking with a cone shaped dock under ocean currents, *Ocean engineering*. Vol. 85, 2014, pp. 110–126.

[5] MSM. Aras,HA. Kasdirin, MH. *Jamaluddin, MF. Basar, of Engineering and Technology, Pro. Malaysian Technical Universities Conference*, Design and Development of an Autonomous Underwater Vehicle (AUV-FKEUTeM), Malaysia, 2009, pp. 1–5.

[6] A. Saeidinezhad, AA. Dehghan, MD. Manshadi, Experimental investigation of hydrodynamic characteristics of a submersible vehicle model with a non-axisymmetric nose in pitch maneuver, *Ocean engineering*. Vol. 100, 2015, pp.26–34.

[7] AD. Madan, MT. Issac, Hydrodynamic Analysis of AUV Hulls Using Semi-empirical

and CFD Approach, *Universal Journal of Mechanical Engineering*. Vol. 5, n. 5, 2017, pp. 137–143.

[8] A. Mitra, JP. Panda, HV. Warrior, The effects of free stream turbulence on the hydrodynamic characteristics of an AUV hull form, *Ocean Engineering*. Vol. 174, 2019, pp.148–158.

[9] A. Phillips, M. Furlong, SR. Turnock, *of Ocean Engineering*, Pro. Oceans 2007, The use of computational fluid dynamics to assess the hull resistance of concept autonomous underwater vehicles, Europe, 2007, pp. 1–6.

[10] P.Rattanasiri, PA.Wilson, AB.Phillips, Numerical investigation of a pair of self-propelled AUVs operating in tandem. Vol. 100, 2015, pp.126–137.

[11] Y. Wang, T. Gao, Y. Pang,Y. Tang, Investigation and optimization of appendage influence on the hydrodynamic performance of AUVs, *Journal of Marine Science and Technology*. Vol. 24, n. 1, pp.297–305, 2019.

[12] NM. Nouri, K. Mostafapour, SH. Hassanpour, CFD Modeling of Wing and Body of an AUV for Estimation of Hydrodynamic Coefficients, *Journal of Applied Fluid Mechanics*. Vol. 9, n. 6, 2016, pp.2717–2729.

[13] V. Mishra, S. Vengadesan, SK. Bhattacharyya, Translational added mass of axisymmetric underwater vehicles with forward speed using computational fluid dynamics, *Journal of Ship Research*. Vol. 55, n. 3, 2011, pp.185–195.

[14] T. Gao,Y. Wang, Y. Pang, J. Cao, Hull shape optimization for autonomous underwater vehicles using CFD, *Engineering applications of computational fluid mechanics*. Vol. 20, n. 1, 2016, pp.599–607.

[15] DF. Myring, A theoretical study of body drag in subcritical axisymmetric flow, *The Aeronautical Quarterly*. Vol. 27, n. 3, 1976, pp.186–194.

[16] P. Jagadeesh, K. Murali, Application of low-Re turbulence models for flow simulations past underwater vehicle hull forms, *Journal of Naval Architecture and Marine Engineering*. Vol. 2, n. 1, 2005, pp.41–54.

[17] P. Jagadeesh, K. Murali, CG. Idichandy, Experimental investigation of hydrodynamic force coefficients over AUV hull form, *Ocean engineering*. Vol. 36, n. 1, 2009, pp.113–118.

[18] Z. Nemouchi, Contribution à l'Etude des Jets Impactant Turbulents Présentant une Courbure des Lignes de Courant plus ou moins Faible, *Phd thesis*, Mentouri Constantine university, Algeria, 2012.

[19] NM. White, A comparison between a simple drag formula and experimental drag data for bodies of revolution, *David W Taylor Naval Ship Research and Development Center Bethesda MD*. 1977.

[20] C. Baker, Estimating drag forces on submarine hulls, *Defence R&D Canada – Atlantic, Report*, DRDC Atlantic CR, 2004.

[21] C. Chin, M. Lau, Modeling and testing of hydrodynamic damping model for a complex-shaped remotely-operated vehicle for control, *Journal of Marine Science and Application*. Vol. 11, n. 2, 2012, pp.150–163.